

Carrier transport in layered nanolaminated films

Aniruddha Konar,^{1, a)} Rajan K. Pandey,¹ and Tamilmani Ethirajan¹
 GLOBALFOUNDRIES, Bangalore, 560045, India.

(Dated: 8 June 2021)

Analyzing *ab-initio* electronic and phonon band structure, temperature-dependent carrier transport in layered Ti_2AlC is investigated. It is found that cylindrical Fermi surface is the origin of the anisotropic carrier effective mass (infinite effective mass along c axis) leading to strong anisotropic (insulator along c axis and metallic along the layer) carrier transport in these films. Using electronic and phonon bandstructures, we develop an analytical model of electron-phonon interaction as well as in-plane carrier conductivity originating from strong inter-valley ($s \rightarrow d$) scattering in Ti_2AlC . We invoke density functional theory to calculate the deformation potential corresponding to acoustic phonon vibration. The calculated deformation potential is in well agreement with the extracted deformation potential value from the transport data. Extracted deformation potential will be useful for prediction of transport quantities for application of these metals at elevated temperatures.

I. INTRODUCTION

Layered nano-laminated ternary carbide and nitride metals known as MAX phases, are emerging new class of materials (metals) that bridge the gap of properties between metals and ceramics¹. Commonly denoted as $\text{M}_{n+1}\text{AX}_n$, these materials are known for their unusual and exotic metallic and ceramic properties²⁻⁴. Here M is a transition metal ($M = \text{Ti}, \text{Cr}, \text{V}$, etc) and A is usually an element from group IIIA or IV, and X is either carbon or nitrogen. These are potential compounds for many emerging applications due to their combined metallic and ceramic properties such as high thermal², and electrical conductivity^{5,6}, high stiffness^{7,8}, oxidation resistance and high damage tolerance and low thermal expansion coefficients². Due to their high conductivity and low friction, these compounds are best suitable to rotating electrical contacts and high temperature applications. Recently, analogous to two-dimensional (2D) semiconductors^{9,10}, 2D transparent metallic layers known as MXenes^{11,12} are realized by chemically removing A species from single layer of MAX compounds. These 2D metallic layers can be suitable materials for electrical contacts in emerging 2D electronics^{10,13} as well as transparent electrodes in photovoltaic devices.

A number of scientific reports exist on the electronic structure calculations¹⁴⁻¹⁷, phase stability¹⁸⁻²⁰, elastic^{21,22} and thermal properties²³ as well as NMR²⁴ studies of these laminated metals. On the contrary, very few experimental reports^{5,6,25,26} is devoted to the transport properties on these metals. Most of the reports assume empirical two band model to explain the experimental observation qualitatively without going into the microscopic details of carrier transport. Though there exists some reports on *ab-initio* studies on electronic structures, no efforts has been made to connect the electronic structures (bandstructure, phonon spectrum, etc) to the mechanism of carrier transport in these systems.

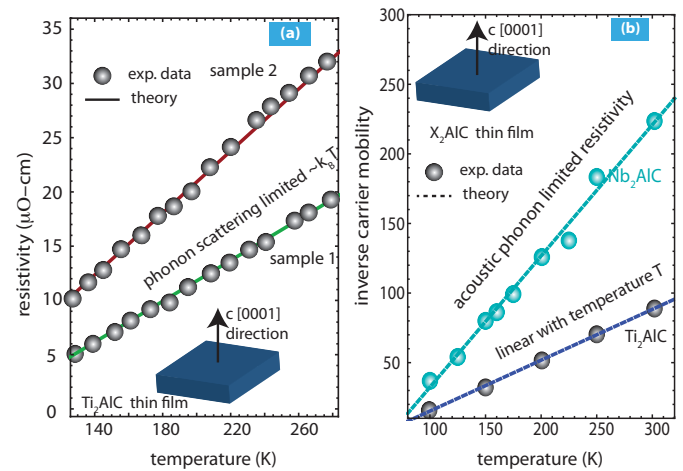


FIG. 1. (a) carrier resistivity function of temperature (data taken from Ref.²⁶) for two different X_2AlC ($X = \text{Ti}$) metal films, (b) measured inverse-mobility (\approx resistivity) data with temperatures of X_2AlC ($X = \text{Ti}, \text{Nb}$, etc) metal films (taken from Ref.⁶) as a function of temperature. Linear fit of temperature-dependent resistivity data indicate electron-phonon interaction limited carrier transport in these laminated metals.

A qualitative approach is made recently²⁶ to explain the anisotropic conductivity in Ti_2AlC , albeit without calculating electron-phonon interaction (assumes a constant scattering time) and phonon spectrum. Here, under deformation potential approximation and Boltzmann transport equation within relaxation time approximation, we develop an analytical expression of conductivity/mobility by carefully analyzing and extracting material parameters from the electronic and phonon spectrum of MAX phase compounds (Ti_2AlC). Using our transport model, the extracted deformation potential values agrees well with the first principle calculations. The developed transport model as well as deformation potential value will be useful for predicting transport properties at elevated temperatures as well as optimizing the performances of devices made out of these laminated metals. Due to

^{a)} Electronic mail: aniruddha.konar@globalfoundries.com

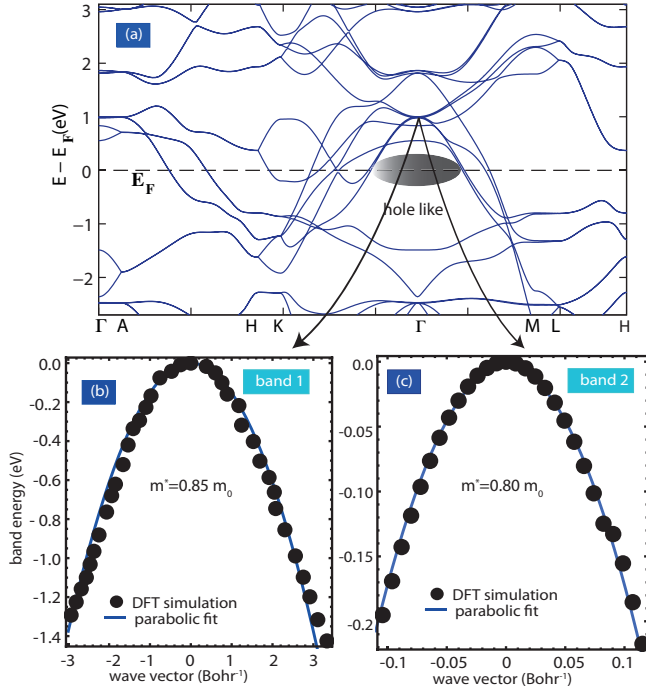


FIG. 2. (a) electronic bandstructure of Ti_2AlC from first principle calculations. Shaded area shows the Fermi level and note that holes are the carrier at the Fermi level. Note that along the basal plane five bands crosses the Fermi level whereas along the c axis ($\Gamma \rightarrow A$) there exists a insulating gap. (b) and (c) effective masses for cylindrical bands.

available of experimental data, we focus only on transport in Ti_2AlC as an illustrative example of MAX phase compound. Similar procedure can be used to explain the measured transport data from electronic and phonon bandstructures of other MAX compounds as well as 2D Mxenes.

II. THEORY AND ANALYSIS

The Fig.1(a) shows the carrier resistivity as a function of temperature for two different Ti_2AlC metal films. It should be noted that the carrier resistivity is increasing with temperature - a typical signature of metallic behavior. In Fig.1(b), we plotted the inverse of mobility (resistivity) for higher temperatures. The linear increase of the resistivity with temperature indicates electron-acoustic phonon scattering limited carrier transport in this metallic system. These different set of measurements convincingly indicates the phonon-dominated carrier transport in these metal films as resistivity is linear with temperature as shown in Fig.1 (linear theoretical fit).

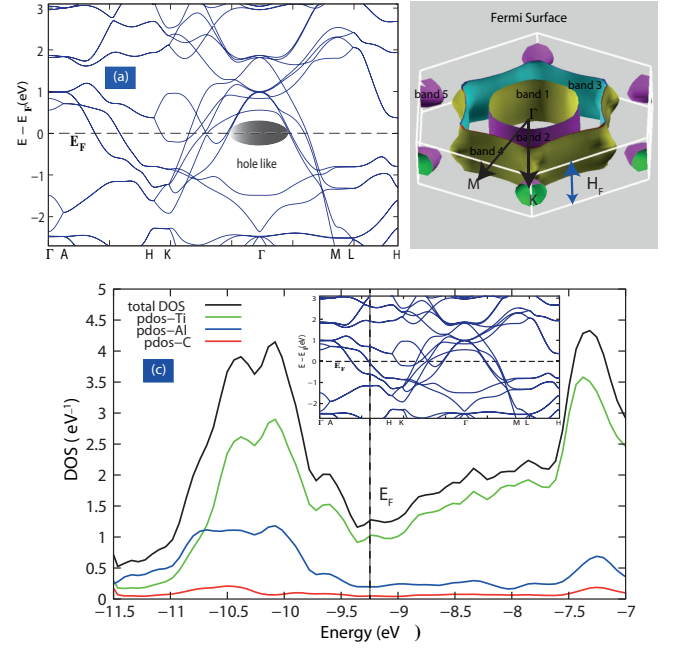


FIG. 3. (a) electronic bandstructure same as Fig.2 (a), and (b) Fermi surface of individual band at the Fermi level. Note that there are five bands at the Fermi level and each of the surface (inner and outer) corresponds to one band. Inner two cylindrical bands responsible of carrier transport in this metal along the basal plane. (c) Total density of states (DOS) as a function of energy. Contributions from each constituent atoms (Ti, Al and C) to the total DOS is plotted with energy. Note that most of DOS at the Fermi level coming from the d-bands of Ti.

A. Electronic Bandstructure

To investigate the transport in these layered metals, it is extremely important to know electronic as well as phonon band structure of the material. We leverage *ab-initio* density functional theory (DFT) to determine electronic structure. Figure 2(a) shows the electronic bandstructure of bulk Ti_2AlC . Density functional theory (DFT) simulations were performed within the local density approximation (LDA), employing Perdew - Zunger (PZ) parameterization of the exchange-correlation functional²⁷ as implemented in the local orbital SIESTA code²⁸. The core and valence electron interactions were treated through pseudopotentials for all the atoms, using Troullier - Martin (TM) method²⁹. Variable cell relaxation was performed till the forces between the atoms were less than 0.02 eV/Å. Calculations have been carried out using a polarized double zeta (DZP) basis with an energy shift of less than 15 meV (0.001 Rydberg). A mesh cutoff of 400 Rydberg and sufficiently fine k-point grid with $18 \times 18 \times 9$ Monkhorst - Pack mesh was used to achieve convergence. Ti_2AlC has a hexagonal crystal structure with lattice parameters: $a = b = 3.0691$ Å, $c = 13.7364$ Å, $\alpha = \beta = 90^\circ$, and $\gamma = 120^\circ$. The fully relaxed crystal within our gener-

ated LDA-TM pseudo potentials has lattice parameters: $a = b = 2.9943 \text{ \AA}$, $c = 13.4519 \text{ \AA}$, $\alpha = \beta = 90^\circ$, and $\gamma = 120^\circ$. These are within 2 - 2.5 percent of the experimental values, which is to be expected as LDA typically underestimates the lattice parameters³⁰.

The anisotropic bandstructure of this layered metal is quite evident from the Figure 2(a). We notice that the system behaves as a metal along the layer (from $\Gamma \rightarrow K$, Fermi level crosses five bands, and from $\Gamma \rightarrow M$, Fermi level crosses four bands), while along the c axis (perpendicular to the layer) it is an insulator (notice that no band crosses the Fermi level along the $\Gamma \rightarrow A$ direction; there exists a virtual band gap along this direction). Moreover, it is evident from the band structure that the transport is hole like along the layer. These hole bands are coming from the d -orbital of the titanium (Ti) atom in the unit cell. Among these bands in the Fermi level, typically holes in the fast-moving bands (bands with steep curvature thus lower effective masses) conduct current. For these bands the cumulative conductivity is written as $\sigma_t = \sum_i \sigma_i = ne^2 [\sum_i \tau_i / m_i^*]$. Here n is the volume carrier density, e is the electronic charge, τ_i is the hole lifetime and m_i^* is the hole effective mass in the i^{th} band. As conductivity is inversely proportional to the effective mass, carriers in the highest curvature band (lower effective mass) carries most of the current. In Fig.2(b) & (c), we have shown the effective mass of two most highest curvature (lowest effective mass) bands with similar effective mass $m^* \approx 0.8m_0$, where m_0 is the free electron mass. It should be note that, the band-edge effective mass definition is only valid for semiconductors, where Fermi level lies close to the conduction band edge. In this case, since the fastest two-bands are radially symmetric (see the Fermi surfaces in Figure 3(b)), effective-mass formalism should be valid.

B. Transport Formalism

Having determined the bandstructure, we now turn into transport calculations in this layered metal. For an applied electric field E (say along x direction), the current in a metal is determined using Boltzmann transport equation. Under relaxation time approximation³¹, the current density can be written as $j_x = -\sigma(T)E$ where $\sigma(T)$ is the carrier conductivity. $f^0(\mathcal{E})$ is the equilibrium Fermi-Dirac distribution function, and \mathcal{E} is the band energy. The carrier conductivity has the form $\sigma(T) = 2g_v \left(\frac{e}{\hbar}\right)^2 \oint_{FS} \left[\left(\frac{\partial \mathcal{E}}{\partial k_x} \right)^2 \frac{\tau(\mathcal{E}_f) dS}{(2\pi)^3 |\nabla \mathcal{E}| \mathcal{E}_f} \right]$, where the surface integration is done on the Fermi surface (FS). Here, e is the change of an electron, \hbar is the reduced Planck constant, \mathcal{E}_k is the band energy of carriers and g_v is the band degeneracy factor. The carrier relaxation time $\tau(k)$ contains the information of electron-phonon scattering in this metal. The electron-phonon relaxation time can be evaluated following Mott's two-band model³³. Here holes from the symmetric fast band scatter to the vacant

states which are coming from the d -orbitals of the Ti. Under the relaxation time approximation, the momentum relaxation due to phonon scattering can be written as $\tau(k)^{-1} = \frac{2\pi}{\hbar} \int_k \frac{d\mathbf{k}'}{(2\pi)^3} |\mathcal{M}_{k,k'}|^2 (1 - \cos \theta) \delta(\mathcal{E}_{k'} - \mathcal{E}_k)$, where k (k') is the initial (final) wave vector of scattering, \mathcal{E}_k ($\mathcal{E}_{k'}$) is the initial (final) carrier energy and θ is the angle of scattering. The matrix element of scattering is given as $\mathcal{M}_{k,k'} = \langle k' | V(r) | k \rangle$, where $\langle k' |$ ($| k \rangle$) is the final (initial) state of scattering and $V(r)$ is the perturbation scattering potential. For long-wavelength crystal vibration (acoustic phonon), the perturbation potential is $V(r) = - \left[\sqrt{\frac{2\hbar}{\Omega \rho \omega_\lambda(q)}} \right] \vec{q} \cdot \vec{e}_\lambda \Xi \left[e^{i(k \cdot r - \omega_q^\lambda t)} + c.c \right]$, where Ω is the unit cell volume, ρ is the mass density, $\omega(q)$ is the phonon frequency, q is the phonon wave vector, \vec{e}_λ is the polarization vector, and Ξ is the acoustic deformation potential³². Denoting carrier Bloch wave function $\langle k | r \rangle = \frac{1}{\sqrt{\Omega}} \mathcal{U}_k(r) e^{i\vec{k} \cdot \vec{r}}$, the electron-phonon scattering rate for longitudinal phonon is written as³⁴

$$\tau(\mathcal{E}_f)^{-1} = \left[\frac{\pi \Xi^2 k_B T}{\hbar \rho v_s^2} \right] N_d(\mathcal{E}_f), \quad (1)$$

where k_B is the Boltzmann constant, T is the lattice temperature, and v_s is the phonon velocity. The entity $N_d(\mathcal{E}_f)$ is the available d -band density of states (available band for scattering in two band model) which are mostly coming from the d -orbital of the Titanium atom. With this prescription of calculating scattering time, it is possible to determine the carrier conductivity for fast moving bands with cylindrical symmetry (band 1 and band 2 in Fig.3(b)). For the band with cylindrical Fermi surface, the energy dispersion can be written as $\mathcal{E}_f = \frac{\hbar^2 (k_F^R)^2}{2m^*}$, for $-H_F/2 \leq k_z \leq H_F/2$, where H_F is the height of the Fermi cylinder in reciprocal space as shown in Fig.3(b). Defining elementary surface on the Fermi cylinder as $dS = k_F^R d\phi dk_z$, where we use cylindrical coordinate system (k_F^R, ϕ, k_z) for the Fermi cylinder and defining the Fermi velocity as $\mathbf{v}_F = \frac{1}{\hbar} \nabla_k \mathcal{E}(k) = \sqrt{2\mathcal{E}_f/m^*} \hat{r}$, the conductivity integral can be simplified to

$$\begin{aligned} \sigma &= \left[\frac{g_v e^2 \tau(\mathcal{E}_f) v_F k_F^R H_F}{(2\pi)^3 \hbar} \right] \int dk_z \int_0^{2\pi} \cos^2 \phi d\phi \\ &= \left(\frac{2e}{\hbar} \right)^2 g_v \tau(\mathcal{E}_f) H_F \mathcal{E}_f = \underbrace{\left(\frac{8m^* \mathcal{E}_f H_F}{\hbar^2} \right)}_{n_h} e \left[\frac{e\tau(\mathcal{E}_f)}{m^*} \right], \end{aligned} \quad (2)$$

where n_h is the hole density and $\mu_h = e\tau(\mathcal{E}_f)/m^*$ is the hole mobility. Since there are two equivalent cylindrical bands, band degeneracy $g_v = 2$. Comparing the above equation with the conventional definition of conductivity $\sigma = ne\mu$, we write the hole density as $n_h = 4m^* \mathcal{E}_f H_F / \hbar^2$. Using the relations $v_F = \sqrt{2\mathcal{E}_f/m^*}$, and $k_F^R = \sqrt{2m^* \mathcal{E}_f}$, we have the following form of hole density $n_h = [(k_F^R/\pi)^2 H_F]$. This is in sharp difference with isotropic elemental metals where Fermi surface

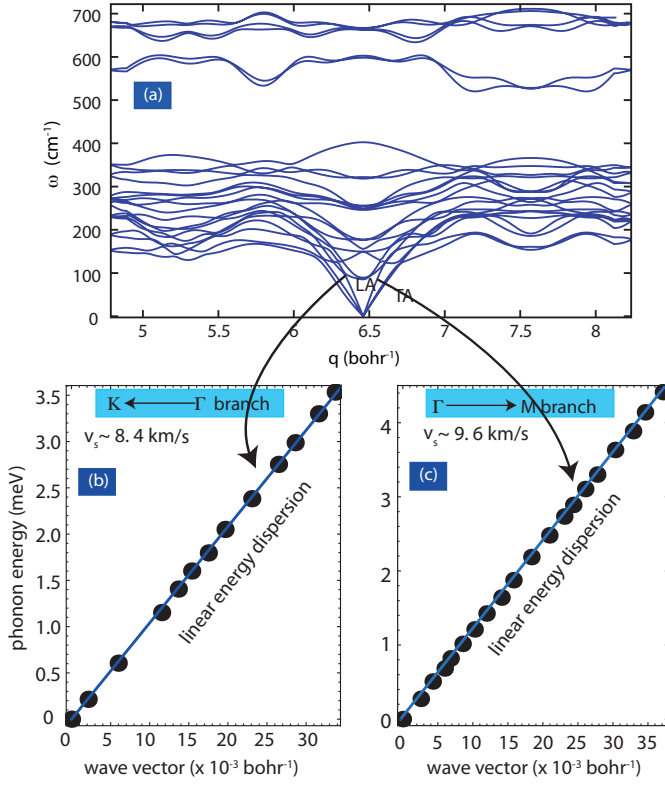


FIG. 4. (a) phonon bandstructure of Ti_2AlC calculated from first principle methods illustrating three low-energy acoustic phonon branches (two transverse modes and one longitudinal mode) and dispersionless optical modes. Longitudinal acoustic modes are fitted with linear dispersion relation $\mathcal{E}_{ph} = \hbar v_s q$ to extract sound velocity shown in (b) & (c).

is rather spherical and the carrier density is given by $n = k_F^3/3\pi^{231}$, where k_F is the average isotropic Fermi wave vector. This stems out from anisotropic bandstructure of these layered materials.

The above two equations pertaining to carrier transport can be compared with experimental observations to extract important transport parameters. To calculate the scattering rate using Eq.1, we need to know few material related parameters which are not a-priori available in literatures. For example, the scattering rate calculation in Eq.1 requires material related parameters such as effective mass, Fermi energy, d-band density of states at the Fermi level, phonon velocity and acoustic-phonon deformation potential energy. Carrier effective mass and Fermi energy are obtained from the ab-initio bandstructure calculation as shown in Fig.2. The total d-band density of states $N_d(\mathcal{E}_f)$ is also obtained from density functional theory calculations as shown in Fig.3(c). Figure 3(c) shows the individual contributions of each constituent atoms to the total density of states. It is evident from the plot that most of the states in the Fermi level are coming from valence d electrons of Titanium. Please note total density of states is plotted in Fig.4, whereas $N_d(\mathcal{E}_f)$ is the density of states per unit volume. Using

the unit cell volume $V_c = 104.45 \text{ Ang}^3$, the density of states at the Fermi energy ($\mathcal{E}_f = -9.24 \text{ eV}$) found to be $N_d(\mathcal{E}_f) = 1.19 \times 10^{28} / \text{eV.m}^3$.

C. Phonon Bandstructure

For the phonon velocity, we perform a ab-initio phonon bandstructure calculations as shown in Fig.4(a). To compute acoustic phonon modes, we employed the technique of frozen phonon method as implemented in SIESTA²⁸. Prior to this, we made sure the convergence of all the ground state properties was achieved, and that the structure was fully relaxed before we carried out phonon band structure calculation. A large enough supercell with as many as 600 atoms was used to ensure sufficient attenuation of real-space force constants.

Since the low-energy acoustic phonon follow the linear dispersion rule, i.e. $\mathcal{E}_{ph}(q) = \hbar v_s q$ (\mathcal{E}_{ph} is the phonon energy and q is the phonon wave vector), by fitting the longitudinal acoustic phonon (LA-phonon) with a linear function, we extract the average phonon velocity $v_s \sim 9 \text{ km/s}$. The linear fitting of LA-phonon mode in two different direction is shown in Fig.4(b) & (c). Using all these calculated parameters values, we compare the calculated temperature-dependent mobility with experimental measurements to extract average deformation potential value for electron-phonon interaction. Since $\tau^{-1}(\mathcal{E}_f) \sim T$, the inverse carrier mobility $\mu^{-1} = [e\tau(\mathcal{E}_f)/m^*]^{-1} \sim T$ as shown in Fig.1. By fitting the linear temperature-dependent inverse mobility (\sim resistivity), we extract the average acoustic-phonon deformation potential to be $\sim 8 \text{ eV}$. Since the scattering is interband scattering (s-type to d-type bands) in two bands models, this value of deformation potential corresponds to the interband deformation potential for electron-phonon scattering. The linear fit of inverse mobility (or resistivity) is shown in Fig.1(a) & (b). To reconfirm this value of phonon deformation potential extracted from transport data, we perform an density functional theory-based computation of phonon deformation potential in this material. We quantify the deformation potential^{35,36} through mimicking the lattice deformation due to phonons by introducing unit strain along one or more lattice parameters, and then tabulate the band structure change. Typically, we look at relative change in the conduction band minimum and the valence band maximum (Fermi energy for a metal). We introduced uniaxial, biaxial, and volume compressive, tensile strain as well as torsional strain to mimic all possible effects. By definition³⁶⁻³⁸ $\delta E = D_A \delta V/V$, where D_A is the deformation potential, δE is the change in the band structure due to applied strain (quantified through DFT), and $\delta V/V$ is the relative change in the volume due to strain. The calculated values of deformation potential $\sim 6-8 \text{ eV}$ are in good agreement with the value we estimated from by fitting the experimental data.

III. CONCLUSION

In conclusions, we have investigated the microscopic origin of carrier transport in layered metals such as Ti_2AlC . Density functional theory is used to determine the electronic as well as phonon bandstructure of this metal. The electronic bandstructure shows an anisotropic behavior of this material - metallic conduction in the basal plane and an insulating gap along the c axis. Using the electronic and phonon bandstructure calculated from first principle, we formulate the electron-acoustic phonon scattering as well as carrier conductivity using Mott's two band approach. Comparing our transport equations with temperature-dependent mobility measurements, we estimate the interband acoustic phonon deformation potential to be around 8 eV. This numbers agrees well with the first principle-based estimation. Though we chose Ti_2AlC as a reference system in this work, using our methodology carrier dynamics and transport parameters can be calculated/predicted for a whole range⁶ of MAX-phase compounds and two-dimensional MXene metals. Our transport formulations and the estimated parameters will be useful in high-temperature application of these layered metals.

- ¹M. Radovic and M. W. Barsoum, *Am. Ceram. Soc. Bull.* **92**, 20 (2013).
- ²M. W. Barsoum, *MAX Phases: Properties of Machinable Carbides and Nitrides*, Wiley VCH, 2013.
- ³Z. M. Sun, *Int. Mater. Rev.* **56**, 143 (2011).
- ⁴M. W. Barsoum, *Prog. Solid State Chem.* **28**, 201 (2000).
- ⁵P. Finkel, M.W. Barsoum, J.D. Hettinger, S.E. Lofland, and H.I. Yoo, *Phys. Rev. B* **67**, 235108 (2003).
- ⁶J.D. Hettinger, S.E. Lofland, P. Finkel, J. Palma, K. Harrell, S. Gupta, A. Ganguly, T. El-Raghy, and M.W. Barsoum, *Phys. Rev. B* **72**, 115120 (2005).
- ⁷M. Radovic, M.W. Barsoum, T. El-Raghy, S.M. Wiederhom, and W.E. Luecke, *Acta Mater.* **50**, 1297 (2002).
- ⁸M.W. Barsoum, T. Zhen, S.R. Kalidindi, M. Radovic, and A. Murugaiah, *Nature Mater.* **2**, 107 (2003).
- ⁹A. Geim and K. Novoselov, *Nature Mater.* **6**, 183 (2007).
- ¹⁰Q. H. Wang, K. Kalanter-Zadeh, A. Kis, J. N. Coleman and M. S. Strano, *Nature* **516**, 78 (2014).
- ¹¹J. Halim, M. R. Lukatskaya, K. M. Cook, J. Lu, C. R. Smith, L. Naslund, S. J. May, L. Hultman, Y. Gogotsi, P. Eklund and M. W. Barsoum, *Chem. Mater.* **26**, 2374 (2014).
- ¹²M. Ghidui, M.R. Lukatskaya, M. Zhao, Y. Gogotsi, M.W. Barsoum, *Nature Mater.* **7**, 699 (2012).
- ¹³S. Kim, A. Konar, W. Hwang, J. H. Lee, J. Lee, J. Yang, C. Jung, H. Kim, J. Yoo, J. Y. Choi, Y. W. Jin, S. Y. Lee, D. Jena, W. Choi, K. Kim, *Nature Comm.* **3**, 101 (2012).
- ¹⁴Y. Zhao, Z. Sun, *Phys. Rev. B* **61**, 12570 (2000).
- ¹⁵G. Hug, E. Fries, *Phys. Rev. B* **65**, 113104 (2002).
- ¹⁶G. Hug, M. Jaouen, M. W. Barsoum, *Phys. Rev. B* **71**, 024105 (2005).
- ¹⁷Y. Mo, P. Rulis, Y. C. Ching, *Phys. Rev. B* **86**, 165122 (2012).
- ¹⁸J. Emmerlich, D. Music, A. Houben, R. Dronskowski, J. M. Schneider, *Phys. Rev. B* **76**, 224111 (2007).
- ¹⁹D. Music, A. Houben, R. Dronskowski, J. M. Schneider, *Phys. Rev. B* **75**, 174102 (2007).
- ²⁰M. Dahlqvist, B. Alling, I. A. Abrikosov, J. Rosn, *Phys. Rev. B* **81**, 024111 (2010).
- ²¹J. Wang, Y. Zhou, *Phys. Rev. B* **69**, 214111 (2004).
- ²²R. Arroyave, M. Radovic, *Phys. Rev. B* **84**, 134112 (2011).
- ²³A. Togo, L. Chaput, I. Tanaka, G. Hug, *Phys. Rev. B* **81**, 174301 (2010).
- ²⁴C. S. Lue, J. Y. Lin, B. X. Xie, *Phys. Rev. B* **73**, 035125 (2006).
- ²⁵M. W. Barsoum, H.-I. Yoo, I. K. Polushina, V. Yu. Rud, T. El-Raghy, *Phys. Rev. B* **62**, 10194 (2000).
- ²⁶V. Mauchamp, W. Yu, L. Gence, L. Piraux, T. Cabioch, V. Gauthier, P. Eklund, S. Dubois, *Phys. Rev. B* **87**, 235105 (2013).
- ²⁷J. P. Perdew and A. Zunger, *Phys. Rev. B* **23**, 5048 (1981).
- ²⁸J. M. Soler, E. Artacho, J. D. Gale, A. Garcia, J. Junquera, P. Ordejón, D. Sánchez-Portal, *J. Phys.: Condens. Matter* **14**, 2745 (2002).
- ²⁹N. Troullier, J. L. Martins, *Phys. Rev. B* **43**, 1993 (1991).
- ³⁰P. Hass, F. Tran, P. Blaha, *Phys. Rev. B* **79**, 085104 (2009).
- ³¹J. M. Ziman, *Theory of Solids*, 2nd Edition, Cambridge University Press, 1995.
- ³²J. Bardeen, W. Shockley, *Phys. Rev.* **80**, 72 (1950).
- ³³N. F. Mott and H. Jones, *The Theory of the Properties of Metals and Alloys*, 1st Edition, Dover, 1936.
- ³⁴The envelope wavefunction $\mathcal{U}_k(r)$ follows the normalization condition $\int_{\Omega} \mathcal{U}_k(r) \mathcal{U}_k^*(r) d\vec{r} = 1$. For long wavelength acoustic phonon, phonon wavelength is much larger than the unit cell dimension. As a result, any integral like $\int_V \mathcal{U}_k(r) \mathcal{U}_k^*(r) f_k(r) d\vec{r}$, where $f_k(r)$ is a slowly varying function (such as long wavelength vibration) can be approximated as $\int_V f_k(r) d^3r \int_{\Omega} \mathcal{U}_k(r) \mathcal{U}_k^*(r) d\vec{r} = \int_V f_k(r) d^3r$. Note that here V is crystal volume and Ω is the unit cell volume.
- ³⁵M. Cardona, N. E. Christensen, *Phys. Rev. B* **35**, 6182 (1987).
- ³⁶C. G. Van de Walle, *Phys. Rev. B* **39**, 1871 (1989).
- ³⁷S. H. Van Wei, A. Zunger, *Phys. Rev. B* **60**, 5404 (1999).
- ³⁸S. Bruzzonea, G. Fiori, *Appl. Phys. Lett.* **99**, 222108 (2011).